Available online at www.sciencedirect.com
SCIENCE DIRECT®
International Journal of Heat and Fluid Flow 24 (2003) 657–668
International Journal of HEAT AND FLUID FLOW
www.elsevier.com/locate/ijhff

Improved film cooling from cylindrical angled holes with triangular tabs: effect of tab orientations

Hasan Nasir, Sumanta Acharya, Srinath Ekkad *

Mechanical Engineering Department, Louisiana State University, Baton Rouge, LA 70803-6413, USA

Received 11 November 2002; accepted 28 April 2003

Abstract

The effect of discrete delta (or triangular)-shaped tabs with different orientations on the film cooling performance from a row of cylindrical holes is investigated. The holes are inclined at 35° along the streamwise direction and the tabs are located along the upstream edge of the holes. Three tab orientations are investigated: (1) tabs placed parallel to the film cooled surface covering a part of the hole; (2) tabs oriented downward at −45°; and (3) tabs oriented upwards at 45°. Measurements were carried out in a low-speed wind tunnel using the transient liquid crystal technique. The mainstream velocity and free-stream turbulence intensity in the low-speed wind tunnel are 9 m/s and 7% respectively and the mainstream Reynolds number based on hole diameter is around 7100. Three blowing ratios of 0.56, 1.13, and 1.7 are tested. Results show that the tabs oriented downwards provide the highest effectiveness at a blowing ratio of 0.56 while the tabs oriented horizontally provides the highest film effectiveness at blowing ratios of 1.13 and 1.7. The higher effectiveness with the tabs is due to the generation of secondary eddies counter-rotating with respect to the kidney pair; these eddies reduce jet penetration and thus increase film-cooling effectiveness. The horizontally oriented tabs produce higher discharge coefficients (lower pressure drop) over the entire range of blowing ratios.

Keywords: Turbines; Cooling; Film; Heat transfer; Tabs

1. Introduction

Film cooling is used extensively in modern gas turbine engines for cooling hot gas path components such as nozzle vanes and turbine blades. In film cooling, cooler air is injected through discrete holes on the blade surface to provide a coolant film that protects the outer blade surface from the detrimental effects of the hot combustion gases. The holes are inclined along the streamwise direction at very shallow angles (around 30°) to provide high cooling effectiveness. Film cooling is highest when the coolant flow hugs the surface and does not penetrate and dissipate in the hot mainstream.

In recent years, several studies have focused on developing techniques to enhance film-cooling effectiveness. These techniques have included compound angle-injection (Ligrani et al., 1994a,b; Sen et al., 1996; Schmidt et al., 1996; Ekkad et al., 1997a,b), shaped-holes (Sen et al., 1996, Schmidt et al., 1996; Gritsch et al., 1998a,b; Reiss and Bolcs, 2000; Wittig et al., 1996), holes with struts (Shih et al., 1999), and tabbed holes (Ekkad et al., 2000). Studies with compound angle injection clearly demonstrate higher film-cooling effectiveness, and greater lateral coverage, but this is associated with the penalty of increased local heat transfer coefficient in the region downstream of the jet. With hole shaping, the hole is diffused in the forward direction or in the lateral direction, and the exit jet-velocity is reduced (maintaining the mass flow rate constant) leading to lower penetration and higher film-cooling effectiveness. Further, lateral diffusion of the holes provides greater lateral coverage. Shaped holes provide 30–50% higher film effectiveness and about 20% lower heat transfer coefficients on the surface compared to a typical cylindrical hole at the same blowing ratio. Tabbed-holes have been shown recently by Ekkad et al. (2000) to produce significant increases (nearly 200%) in the film-cooling effectiveness. This improved performance is related to the generation of vorticity by the tabs that counters the kidney-pair vortex of the coolant jets, and

* Corresponding author. Tel.: +1-225-388-5901; fax: +1-225-388-5924.
E-mail address: sekkad1@1su.edu (S. Ekkad).

0142-727X/$ - see front matter © 2003 Elsevier Inc. All rights reserved.
doi:10.1016/S0142-727X(03)00082-1

Nomenclature

C_d	film hole discharge coefficient
d	film hole diameter, cm
DR	coolant-to-mainstream density ratio, ρ_c/ρ_∞
h	heat transfer coefficient with film injection, W/m^2 K
h_0	heat transfer coefficient without film injection, W/m^2 K
I	coolant-to-mainstream momentum flux ratio, $(\rho U^2)_c/(\rho U^2)_\infty$
k	thermal conductivity of test surface, W/m K
k_a	thermal conductivity of air, W/m K
M	blowing ratio, $(\rho U)_c/(\rho U)_\infty$
Pr	Prandtl number
Re	Reynolds number, $\rho U_\infty d/\mu$
t	time of liquid crystal color change, s
T	temperature, K
Tu	free-stream turbulence intensity, $\sqrt{u'^2}/U_\infty$
u'	streamwise velocity fluctuation
U	flow velocity, m/s
X	streamwise distance, m
y	spanwise distance, m
α	thermal diffusivity of test surface, m^2/s
γ	streamwise angle of film hole
η	film effectiveness
μ	fluid dynamic viscosity
ρ	fluid density
Φ	overall cooling effectiveness, $\frac{T_g-T_w}{T_g-T_c}$

Subscripts

c	coolant
f	film
g	gas (real engine)
i	initial
∞	mainstream
w	wall

reduces jet penetration keeping the coolant jet closer to the blade surface. Ekkad et al. (2000) investigated various tab locations and the tab located at the upstream edge of the hole was shown to have the best performance. However, only horizontal tab orientations (tab parallel to the surface) were considered.

There have been several studies in the literature reporting velocity measurements from vertical jets with tabs located at the exit of the jet. A study by Bradbury and Khadem (1975) was the first to focus on the effect of tab placements on vertical jet-cross-flow mixing for orthogonal injection. They placed square tabs and examined the effects on the mixing phenomenon in the flow field downstream of the holes. Zaman and Foss (1997) and Zaman (1998) also placed delta shaped vortex generators upstream of the hole and investigated their effects on the downstream flow field. They reported a 40% reduction in jet penetration. Their tab was triangular in shape and placed such that the apex of the triangle was tilted either up or down into the jet hole exit. They also observed more lateral spreading for the downward tilted tab. However, all the above studies on using tabs were performed on jets with normal injection. Also, only flow field measurements were presented without any information on the effect of tabs on the heat transfer and film-cooling effectiveness.

Most turbine blade geometries typically use angled injection to improve the benefits of film cooling and information on surface heat transfer and cooling effectiveness are important for blade designers. As noted earlier, the only study where the effect of tabs on film-cooling performance has been studied is that of Ekkad et al. (2000) who examined the effect of placing discrete tabs on injection holes angled at 35° along the streamwise direction. The tabs were located along either the upstream edge or the downstream edge of the hole or symmetrically along the spanwise edges. It was observed that placing the tabs along the upstream edge of the hole increased the film-cooling effectiveness over the plain cylindrical hole case. The other tab locations showed no significant improvements in film-cooling effectiveness.

The present study aims to explore the effect of upstream tab orientations on the film-cooling behavior. The tabs are located along the upstream edge of the film-cooling holes since, as noted above, only this location yielded improvements in film-cooling effectiveness. Three tab orientations are examined: (1) parallel to the surface (2) oriented downwards at −45° and (3) oriented upwards at 45°. Of specific interest is to find the tab orientation that provides the highest film-cooling effectiveness and the lowest pressure drop. The hole discharge coefficient or the pressure drop is an important parameter in coolant hole designs and must be considered along with film-cooling effectiveness.

The tests are conducted on a flat surface with a single row of inclined cylindrical holes in a low-speed wind tunnel. Heat transfer measurements are made using a transient liquid crystal technique (Ekkad et al., 1997a,b). The transient liquid crystal technique has several advantages over other techniques such as naphthalene sublimation and steady state techniques. The experimental method is quick, provides high resolution data and the coating is reversible so that it can be reused for several tests. Flow and pressure measurements are made using hot-wire anemometry and pressure transducers respectively.

2. Experimental setup and procedure

All the experiments were carried out in a low-speed wind tunnel setup with compressed air supply for coolant air. Fig. 1 shows the comprehensive view of the experimental arrangement. The test setup consists of a blower connected to a 12 kW heater that heats the air to a free-stream temperature of 58 °C. The air is then routed through a section with baffles to ensure adequate mixing of the hot air to obtain a uniform temperature across the cross-section. The heated air is passed through a 4:1 2-D converging nozzle. In order to allow the air to heat up to the desired temperature, the air exiting the nozzle is initially routed out away from the test section by using a by-pass gate. The temperature of the air is continuously monitored at the exit of the gate, and when the desired temperature is reached, the gate is fully opened. The open gate allows the flow into a test section made of Plexiglas and has a cross-section of 30-cm width and 9-cm height. The components upstream of the test section are covered with insulation to minimize the heating time. The bottom plate of the test section is made of 2.22-cm thick Plexiglas. This plate has a replaceable section about 25.4 cm downstream of the test section inlet. This replaceable section can be interchanged to change the hole geometry. A trip (rod of diameter 0.3175 cm) is placed at the entrance to the test section to ensure the beginning of a new boundary layer. The film holes are located 30.5 cm downstream of the trip. The coolant air is provided from a separate compressed air supply and is metered for flow measurement. The coolant air is then passed through a heater to heat up the air. Prior to the experiment, the hot air is routed away from the test section using a three-way diverter valve. When the valve is flipped, the coolant enters a plenum below the test plate and is then ejected through the film-cooling holes into the test section. The mainstream hot air is flipped a second or so later to allow for coolant to fill the plenum underneath the test plate. The time difference between the switching of coolant and mainstream flow depends on the blowing ratio of the coolant. Thermocouples are mounted upstream of the hole row to measure the mainstream temperature, and inside one of the holes to measure the coolant exit temperature. The image processing system is triggered to initiate taking data only when the mainstream air is diverted into the test section.

Fig. 2 shows the test plate with film hole geometry used in this study. There are six holes of 1.27-cm diameter in each row inclined at 35° in the streamwise direction. The hole spacing between adjacent holes is 3-hole diameters for all the holes. Measurements were performed for the middle four holes. Fig. 3 shows the coolant flow loop and the tab configuration. The tab is a thin equilateral triangle made of cardboard material. Each side of the triangular piece is 1.27-cm and the height of the tab (l) is 1.1 cm. The tabs are placed in the locations as shown in the figure. Case 1 is the plain cylindrical hole with no tabs. In Case 2, the tab is placed on the upstream side of the hole with the tab covering 33% ($3l/4$) of the upstream centerline length of the hole. The tab region projecting over the coolant hole is oriented downwards at 45° ($\theta = -45°$). In Case 3, the tab is oriented parallel to the film cooled surface ($\theta = 0°$). In Case 4, the tab is oriented upwards at 45° ($\theta = 45°$).

Measurements of the free-stream velocity and turbulence were obtained using a calibrated single hot wire and a TSI data acquisition system. These measurements were performed along the jet-centerline at several streamwise locations, and provide information on how

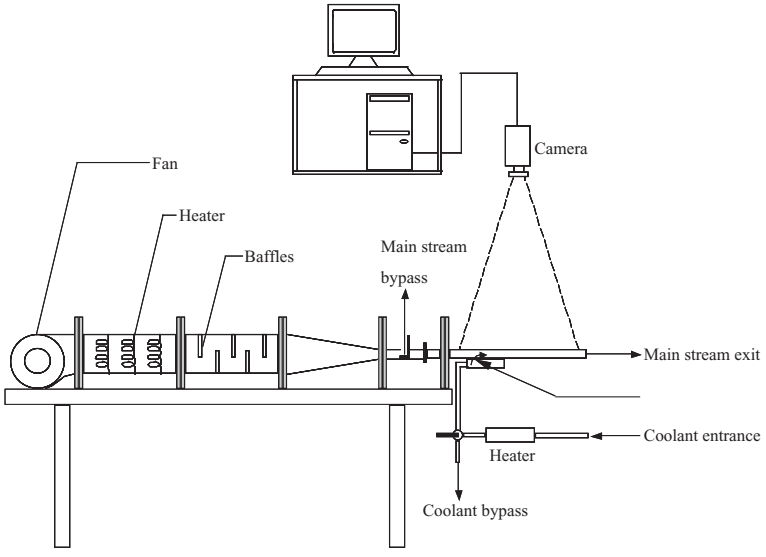

Fig. 1. Experimental setup.

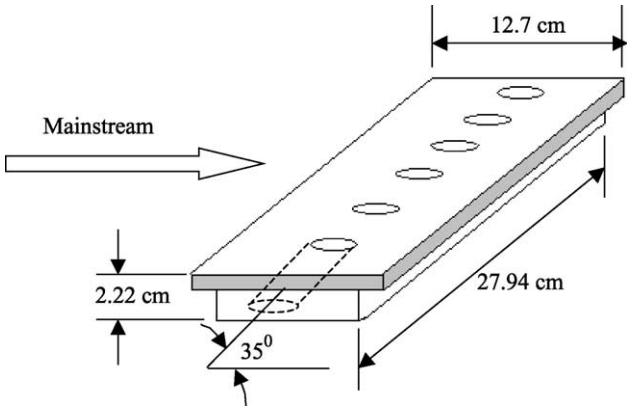

Fig. 2. Test plate geometry.

the tabs influence the jet penetration and jet-cross-flow mixing. These hydrodynamic effects play an important role in determining the cooling effectiveness and heat transfer coefficient. All the hot wire measurements were made for cold flow ensuring there was no temperature contamination of the hot wire results.

The liquid crystal color changes were determined using an image processing system. The RGB camera is placed above the test section and is connected to the Color Frame Grabber board inside the computer. The frame grabber board is programmed through commercially available software to monitor the color change times of the liquid crystal coating. The software tracks the appearance of the green color at every pixel location during a sudden transient heating experiment. Two similar tests are run to resolve the heat transfer coefficient and film effectiveness at every pixel location. An 8-channel A/D system is used for measuring the temperatures during the transient test.

The first test has the mainstream heated to 58 °C and the coolant heated slightly above room temperature. Both the flows are initially heated and routed away from the test section. The airflow is suddenly switched to start a transient heating of the liquid crystal coating. The image processing system and the temperature measurement system are triggered to start obtaining data at the same instant the flows are switched. The time of color change of each pixel location to change color to green since the initiation of the transient test is determined. The second test is run similarly with the coolant temperature heated to a temperature slightly above the mainstream temperature. For this study, there are 400 points along the streamwise direction and 200 points along the lateral direction. A spanwise region of four middle rows is measured with the streamwise distance about 17 hole diameters downstream of the hole downstream edge.

The generalized equation for the three-temperature problem using semi-infinite solid assumption and 1-D transient conduction model is given as,

$$T_w - T_i = \left[1 - \exp\left(\frac{h^2\alpha t}{k^2}\right)\mathrm{erfc}\left(\frac{h\sqrt{\alpha t}}{k}\right)\right] \times [\eta T_c + (1-\eta)T_\infty - T_i]$$

where T_w is the liquid crystal color change temperature (35.4 °C). The transient responses of the mainstream and coolant temperatures during the tests are incorporated using the Duhamels' superposition theorem. Subsequently, the two equations with different coolant temperatures and color change times are solved simultaneously to determine the local heat transfer coefficient and film effectiveness values at every single point on the test surface. More details of this solution technique are presented by Ekkad et al. (1997a,b).

As shown by Ekkad et al. (1997b), the local heat flux ratio q''/q''_0 , the heat flux with film injection to that without film injection can be expressed as

$$\frac{q''}{q''_0} = \frac{h}{h_0}\left(1 - \frac{\eta}{\Phi}\right)$$

where h/h_0 and η is the area averaged heat transfer coefficient and film effectiveness values respectively. The value of Φ is the overall cooling effectiveness. A value of 0.6 was assumed for the overall cooling effectiveness for

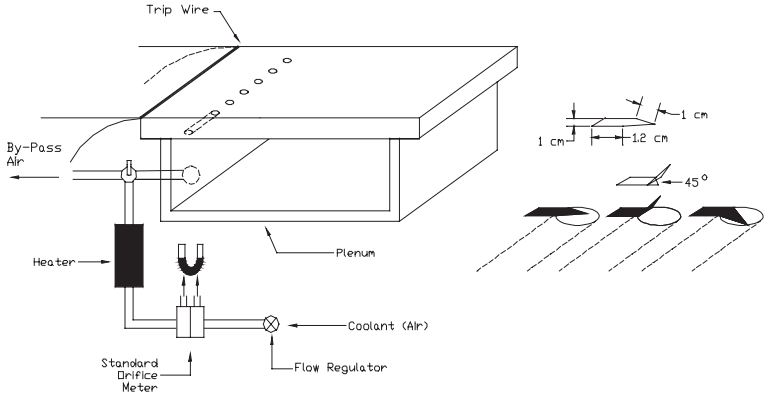

Fig. 3. Film hole and flow geometry and tab configuration.

this study. A heat flux ratio of less than 1.0 indicates that film injection reduces the heat flux into the surface.

Experimental uncertainty in heat transfer coefficient and film effectiveness measurement is estimated to be about ±6.4% and ±7.9%, respectively using the methodology of Kline and McClintock (1953). The individual uncertainties in color change time (t) is ±0.2 s; mainstream temperature (T_∞) is ±0.2 °C; surface initial temperature (T_i) is ±0.5 °C; coolant temperature (T_c) is ±0.2 °C; and material physical properties ($\sqrt{\alpha/k}$) is ±3%. Near hole, the results are affected by two-dimensional conduction. This issue is not critical to the heat transfer coefficient distributions as both coolant and mainstream are heated for the hot test. However, it should be noted that the over-prediction in the immediate vicinity of the film hole for film effectiveness could be as high as 17%. The above estimated levels in uncertainty near the holes are due to the possibility of invalidation of the semi-infinite model assumption. Experimental uncertainty is the flow velocity and turbulence intensity measurements are in the order of ±4%.

3. Results and discussion

The measured mainstream velocity and free-stream turbulence intensity using a calibrated single hot wire probe are 9 m/s and 7%, respectively. The mainstream Reynolds number (Re_d) based on film hole diameter is 7100. The boundary layer profile measured downstream of the trip is close to the fully turbulent flow profile (1/7th law). The momentum thickness Reynolds number (Re_θ) just upstream of the hole is 511 and the corresponding boundary layer thickness is 9.87 mm. Three blowing ratios, $M = 0.56$, 1.13, and 1.7, are investigated in this study.

3.1. Velocity measurements

Fig. 4 presents the velocity profiles upstream of the hole ($X/d = -1$) and at several locations downstream of the hole ($X/d = 1$, 3, 5, 10). These velocity profiles are presented for a representative $M = 1.13$. The upstream velocity profile is unaffected by the jet injected into the boundary layer downstream. The oncoming velocity profile, as indicated earlier, is typical of a turbulent boundary layer with 1/7th law profile. The no-tabs (Case 1) velocity profile shows an inflection due to the coolant jet just downstream of injection at $X/d = 1$ with the highest velocity around $Y/d \sim 0.8$. Further downstream, the jet injection effect reduces rapidly, and the flow begins to recover. However, even at $X/d = 10$, the velocity profile indicates that the flow recovery is not yet complete. For the straight or horizontal tab (Case 3), the location of peak velocity is closer to the wall ($Y/d \sim 0.6$) indicating that the jet penetration is reduced in the

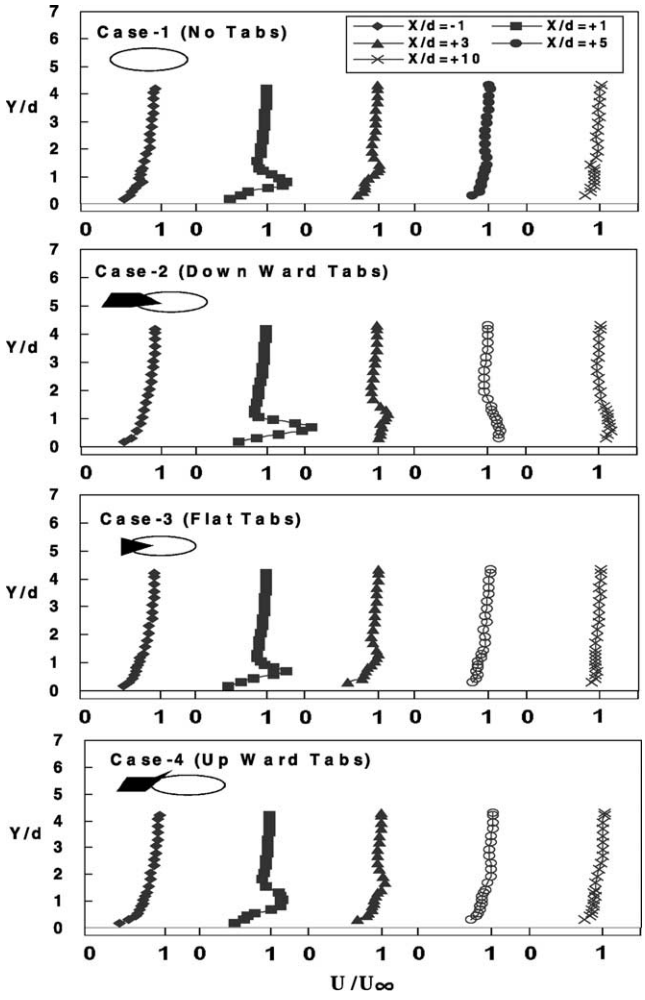

Fig. 4. Velocity profiles upstream and downstream of film injection.

presence of the horizontal tabs. With the tabs located upstream of the hole center, a vortical pair with vorticity opposite to that of the jet-kidney vortices are obtained (Zaman, 1998) and reduce the strength of the kidney vortices. This reduces the self-induction of vorticity and the jet penetration. This should lead to improved film-cooling effectiveness (presented in the next section). The lower jet penetration can also be observed at $X/d = 3$. For the downward tab (Case 2), the jet is again closer to the wall (peak velocity location at $Y/d \sim 0.6$) than for the no-tab case and the coolant jet velocity at $X/d = 1$ is higher than for all the other cases. As far downstream as $X/d = 10$, the coolant jet seems to stay close to the wall in contrast to the other cases. This behavior is again conducive for cooling effectiveness. With the upward tab (Case 4), the peak-velocity at $X/d = 1$ occurs at a higher Y/d location ($Y/d \sim 1$–1.1). This is also evident in the velocity profile at $X/d = 3$ where the peak velocity location is shifted upwards relative to the location for the no-tabs case. The upward deflection may be due to a Coanda effect by which the jet is pulled toward the

upward oriented tab. The greater jet penetration is expected to be detrimental for film-cooling effectiveness.

Fig. 5 presents the turbulence intensity upstream ($X/d = -1$) and at several locations downstream of the hole ($X/d = 1, 3, 5, 10$). Several studies have shown that jet injection produces increased turbulence levels inside the boundary layers due to the shear layer mixing and this is the main reason that the local heat transfer coefficients downstream of jet injection show higher values. To improve blade cooling, the cooling effectiveness must be increased without affecting the surface heat transfer coefficients. The profiles in Fig. 5 show two peaks, and represent the wake-region (peak closer to the wall) and the jet (peak closer to the free-stream). The effect of these separate origins can be seen as far downstream as $X/d = 5$. Note that the cross-flow boundary layer is entrained into the wake downstream of the jet injection, and is responsible for the high turbulence intensities observed in this region. In Fig. 5, the maximum turbulence intensities will be interpreted as a measure of the enhanced turbulent mixing produced by the tabs. For the no tabs condition (Case 1), the maximum turbulence intensity at $X/d = 1$ is around 25%. The turbulence intensity for the horizontal or straight tab is slightly higher than that for the no tab conditions (Case 3) indicating that the presence of the tab does not considerably enhance the shear layer mixing. However, as pointed out earlier in the velocity plots, the jet is closer to the surface (note that the location of the coolant jet is harder to discern in the turbulence intensity plots due to the high turbulence values in the wake). The greater proximity of the jet to the wall is likely to lead to enhanced effectiveness as seen later. Further the slight increase in the intensity levels, and the greater proximity of the peak velocity to the wall is also likely to increase the heat transfer coefficient. The turbulence intensity for the downward tab (Case 2) is much higher with values close to 40%. The jet is also close to the surface for this case (relative to Case 1), as seen earlier, in the mean velocity profiles. Therefore both high effectiveness and high heat transfer coefficients are expected for this case. The turbulence intensity decreases for the upward tabs (Case 4). However, as for the mean velocity, the location of the peak turbulence intensity is shifted away from the wall. The upward shift in the peak velocity and turbulence intensity locations is likely to reduce film-cooling effectiveness, while the reduced turbulence intensity levels themselves are likely to reduce heat transfer coefficient.

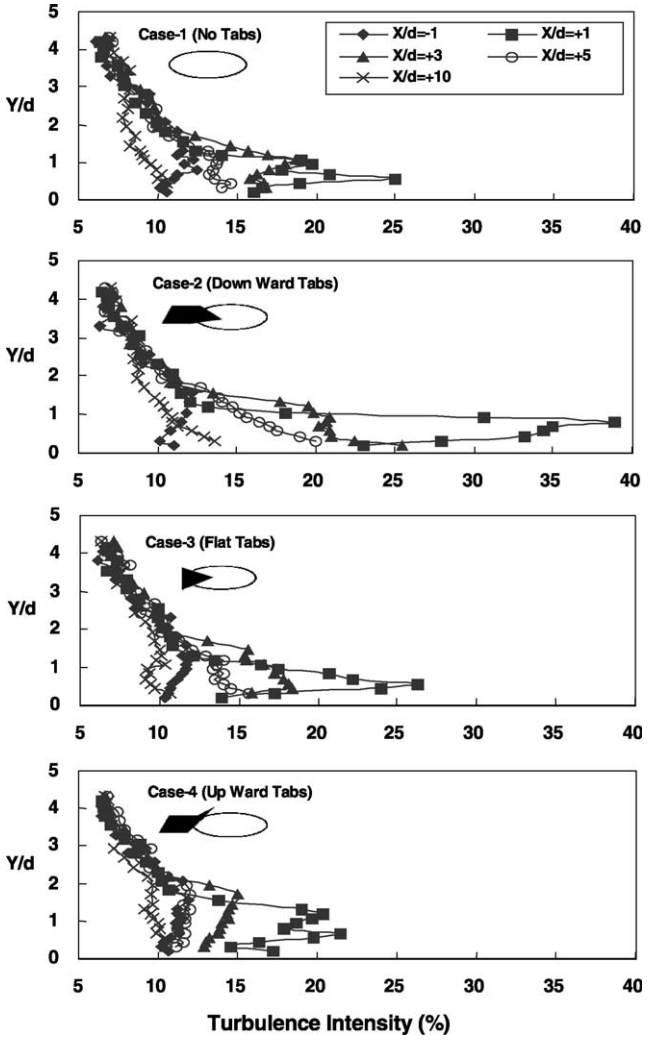

Fig. 5. Turbulence intensity distributions upstream and downstream of injection.

3.2. Film-cooling effectiveness and heat transfer coefficient

Fig. 6 presents the comparison of the present results with published results for $M = 1.13$ for simple injection holes (Case 1). The spanwise averaged film effectiveness ($\overline{\eta}$) results for $M = 1.13$ are compared with the results from Pedersen et al. (1977) at $M = 1.0$, Schmidt et al. (1996) at $M = 1.25$, and Gritsch et al. (1998b) at $M = 1.0$ in Fig. 6(a). Results show that the present data for $M = 1.13$ is in good agreement with results from all the above studies. The data from Gritsch et al. (1998b) also shows the slight increase in film effectiveness just downstream of the holes. Other studies do not present data close to the hole. The spanwise averaged heat transfer coefficient ratios ($\overline{h}/h_0$) for $M = 1.13$ are plotted versus the normalized axial distance from the hole (X/d) in Fig. 6(b), and compared with the studies by Eriksen and Goldstein (1974) at $M = 1.0$, Hay et al. (1985) at $M = 1.0$, and Gritsch et al. (1998a) at $M = 1.5$. Based on the above comparisons, it is fair to say that the results from the present study are in good agreement with published results for the baseline case, Case 1.

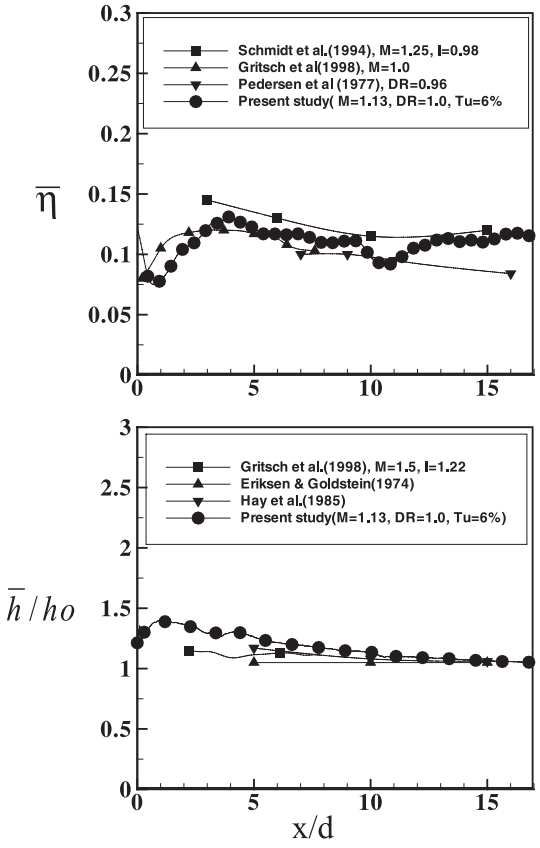

Fig. 6. Comparison of present data with other studies.

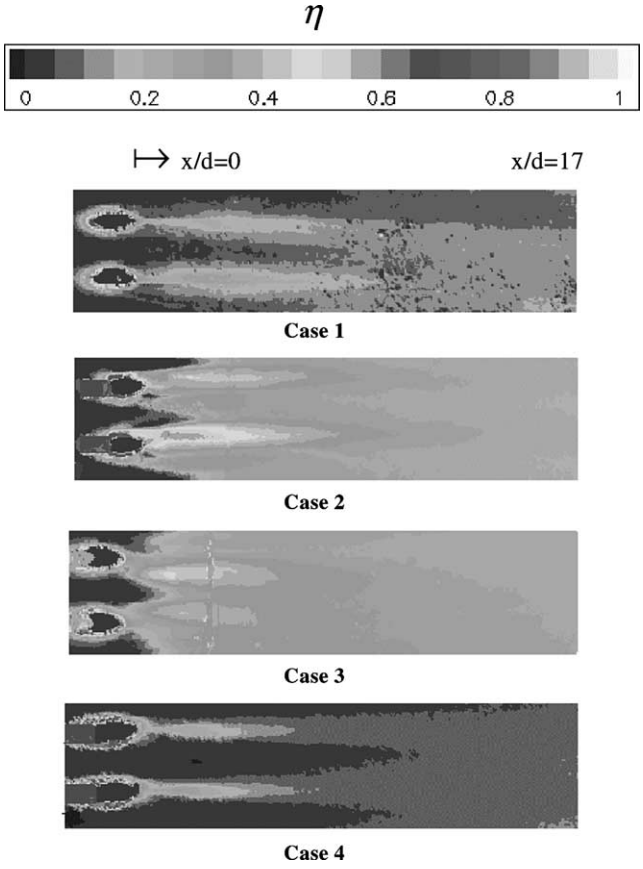

Fig. 7. Detailed film effectiveness distributions for all cases, $M = 1.13$.

Fig. 7 presents the detailed film-cooling effectiveness distributions (η) for all cases at $M = 1.13$. The detailed distributions are shown for only the two middle holes although measurements were performed for the middle four holes. For Case 1 (no tabs), the film effectiveness distributions are higher along the jet centerlines, with almost no cooling in between the holes for most of the plate length. The jets appear to lift off at the downstream edge and reattach farther downstream creating a low effectiveness region just downstream of the holes. After reattachment, the jets spread laterally and full spanwise coverage is observed around $X/d = 8$. Case 2 (tabs with $\theta = -45°$), shows much higher effectiveness than Case 1 over the entire region. Further, complete coverage is achieved within 2-hole diameters. For this case, as noted earlier in Fig. 4, the jet was closest to the surface and is therefore responsible for the high effectiveness. The rapid lateral increase in the coverage is indicative of enhanced coolant jet coverage in the lateral direction. Case 3 (tabs with $\theta = 0°$) shows enhancements in film-cooling effectiveness similar to those of Case 2 with slightly lower effectiveness values in the near vicinity of the hole. In this case, the coolant jet penetration was again reduced by the tabs (Fig. 4), and this fact is again responsible for the improved film-cooling effectiveness. However, the higher turbulence intensity levels observed for this case are perhaps responsible for greater mixing and lower effectiveness than Case 2. The film-cooling effectiveness for Case 4 (tabs oriented upward with $\theta = 45°$) is quite low, and is even lower than the baseline case with no tabs. This is because the tabs oriented upwards at 45° do not interact with the jet in the same manner as the tabs in Cases 2 and 3, and therefore the tabs do not generate the vortex pair produced by the downward oriented or horizontal tabs. Instead, as shown earlier, the jet penetration is enhanced in this case presumably due to a Coanda-type effect. This enhanced penetration leads to lower effectiveness. The upward oriented tabs also interacts with the cross-flow, and deflects it around the jet holes. Thus the blanketing effect of the cross-flow pushing the jet downward is diminished leading to reduced coverage of the surface by the coolant film. Further since the upward tabs provide partial blockage to the cross-flow, the deflected flow is accelerated between the coolant holes, diminishing the lateral spreading of the jets.

Fig. 8 presents the detailed heat transfer coefficient ratio distributions (h/h_0) for all cases at $M = 1.13$. The baseline heat transfer coefficient (h_0) was measured on the test plate without film holes. The heat transfer

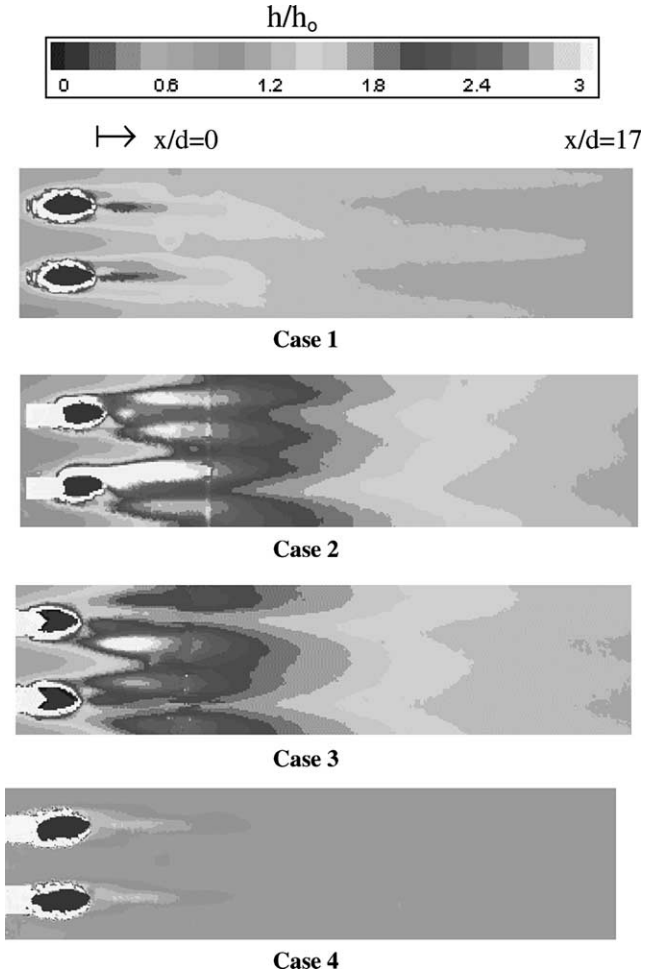

Fig. 8. Detailed heat transfer coefficient ratio distributions for all cases, $M = 1.13$.

coefficient distributions for the Case 1 holes clearly show the presence of the counter rotating vortex pair with heat transfer coefficients higher along the side edges of the hole. The results are consistent with that presented by Goldstein and Taylor (1982). The region along the centerline shows a low heat transfer region behind the downstream edge of the hole. This is potentially due to the action of jet lift-off and flow separation downstream of the jet. Further downstream, the heat transfer coefficient ratio is enhanced beyond values of 2.0. As for the film-cooling effectiveness, Cases 2 and 3 show similar behavior and exhibit much higher heat transfer coefficient ratios compared to Case 1. As noted earlier, the tab-induced vorticity reduces the jet vertical penetration and also increases the turbulence levels. The increased turbulence levels are responsible for the greater levels of heat transfer coefficient. In Fig. 5, Case 2 shows higher peak turbulence levels than Case 3, and correspondingly, higher heat transfer coefficients are observed for Case 2 in Figs. 8 and 9. Case 4 shows lower heat transfer coefficient ratios and also lesser spreading than Cases 2 and 3. In fact the heat transfer coefficient values for Case 4 are lower than those of Case 1. This observation is again linked to the lower turbulence intensity levels obtained in Case 4 (Fig. 5).

Fig. 9 presents the effect of blowing ratio (M) on the spanwise averaged film effectiveness ($\overline{\eta}$) and heat transfer coefficient ratio ($\overline{h}/h_0$) distributions for the four cases considered. For all four cases, the film effectiveness is highest for $M = 1.13$ over most of the test section. In general, the best results for effectiveness are obtained for Cases 2 and 3 due to the reduced jet penetration (Fig. 4) obtained for these cases. Peak values of around 0.35 are achieved for Cases 2 and 3 roughly 3-hole diameter downstream of injection. Except for Case 3, effectiveness is lowest for $M = 1.7$ presumably due to greater vertical penetration of the jet. As note earlier, Case 4 shows no increase in effectiveness over Case 1. The highest effectiveness is around 0.17 for this hole geometry at any blowing ratio.

As expected, the heat transfer coefficient ratios increase with increasing blowing ratio. The increased coolant injection typically produces increases in mixing and turbulence generation resulting in higher heat transfer coefficients. Comparing the four cases it is evident that Case 2 has the highest heat transfer coefficient and is correlated to the highest turbulence intensity values obtained for this case (Fig. 5). Analyzing the effectiveness and heat transfer coefficient values together, it is evident that for Case 2, best performance (highest effectiveness, lowest heat transfer coefficient) is achieved at $M = 0.56$, while the worst performance (lowest effectiveness, highest heat transfer coefficient) is observed at $M = 1.7$. For Case 3, increasing effectiveness is associated with increasing heat transfer coefficient. At $M = 1.13$ and 1.7, Case 3 appears to exhibit higher effectiveness values but lower heat transfer coefficients than Case 2, and would appear to be the best choice from a cooling perspective.

Fig. 10 presents the effect of tab orientation on spanwise averaged film effectiveness ($\overline{\eta}$) and heat transfer coefficient ratio ($\overline{h}/h_0$) for the three blowing ratios considered. Effectiveness is generally highest at $M = 1.13$ and drops off as M is increased to 1.7 presumably due to jet lift-off. For Cases 1, 2 and 4, the drop in the effectiveness values at $M = 1.7$ is generally greater than 50%, while there is only a marginal decrease in effectiveness for Case 3. This clearly indicates the capability of the horizontal tabs (Case 3) in effectively reducing jet penetration through the introduction of vorticity counter to the kidney pair. However, it should be noted that even with the reduced effectiveness at $M = 1.7$, Cases 2 and 3 have higher peak effectiveness values (0.15 and 0.3 respectively) compared to the baseline case. Clearly, if superior performance in terms of effectiveness is required over a range of blowing ratios, Case 3 with

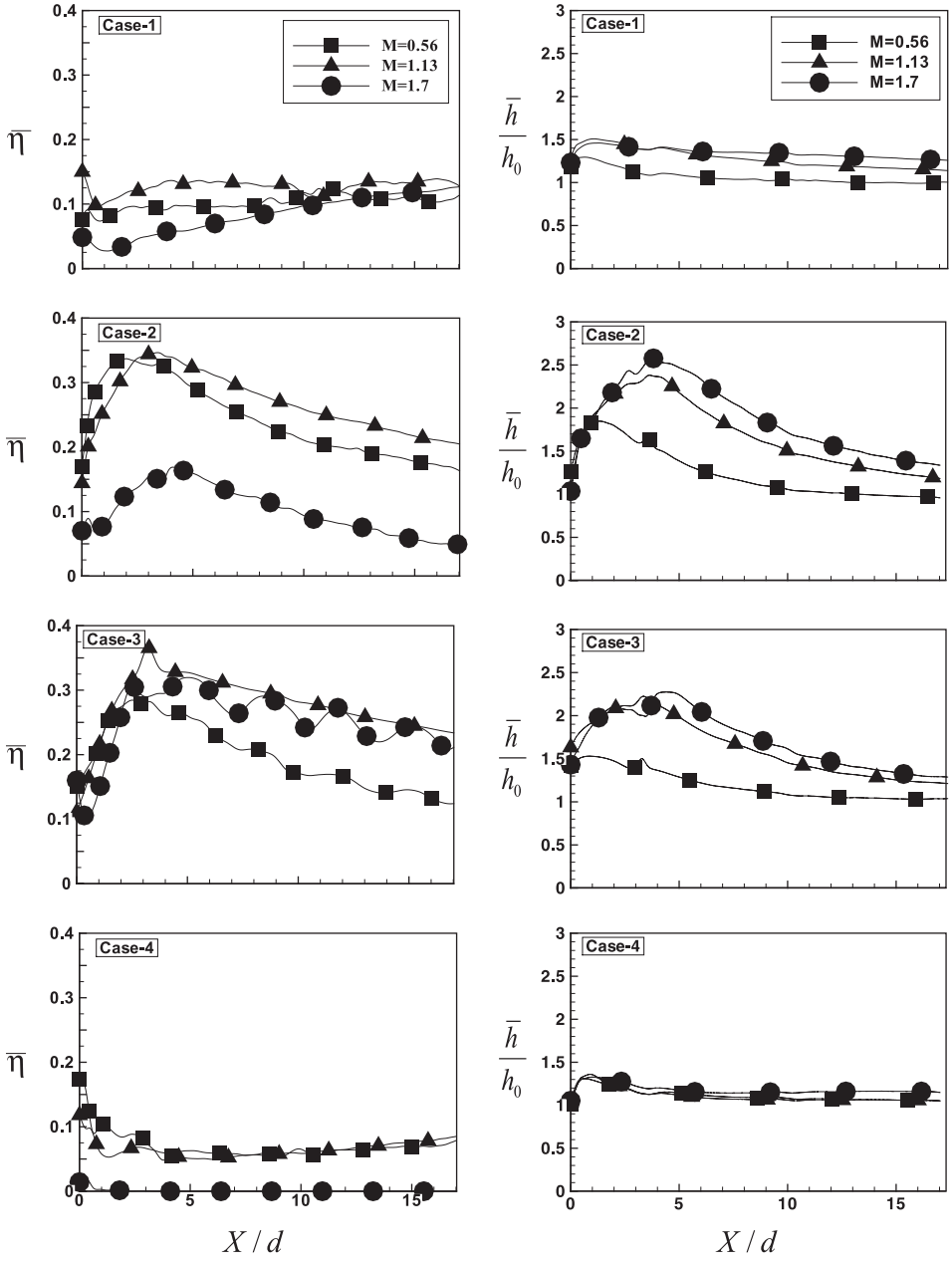

Fig. 9. Effect of blowing ratio on span averaged film effectiveness and heat transfer coefficient ratio distributions for all tab orientations.

horizontal tabs is the most desirable; on the other hand, Case 2 performs at the same level as Case 3 at $M = 0.56$ and 1.13. Case 4 is clearly unacceptable since the effectiveness values are even lower than the baseline cylindrical case.

The average heat transfer coefficient distribution for Cases 2 and 3 increase with blowing ratio and the location of the peak shifts downstream. The increase in the average heat transfer coefficient occurs primarily from $M = 0.56$ to 1.13, with the peak location shifting from immediately downstream of the hole at $M = 0.56$ to $X/d = 4$ at $M = 1.13$. This shift in the peak is due to jet lift-off and reattachment at the higher blowing ratio. From $M = 1.13$ to 1.7, no significant change in heat transfer coefficient is observed; contrast this with the significant reduction in effectiveness for Case 2 when M was increased from 1.13 to 1.7. For Cases 1 and 4, the changes in heat transfer coefficient with M are rather small.

Fig. 11 presents the effect of momentum flux ratio (I) on area-averaged (or overall-averaged) heat transfer coefficient ratios ($\overline{\overline{h}}/h_0$) and film effectiveness ($\overline{\overline{\eta}}$) for each of the four cases. Momentum flux ratio is used as it encompasses the density ratio and blowing ratio into

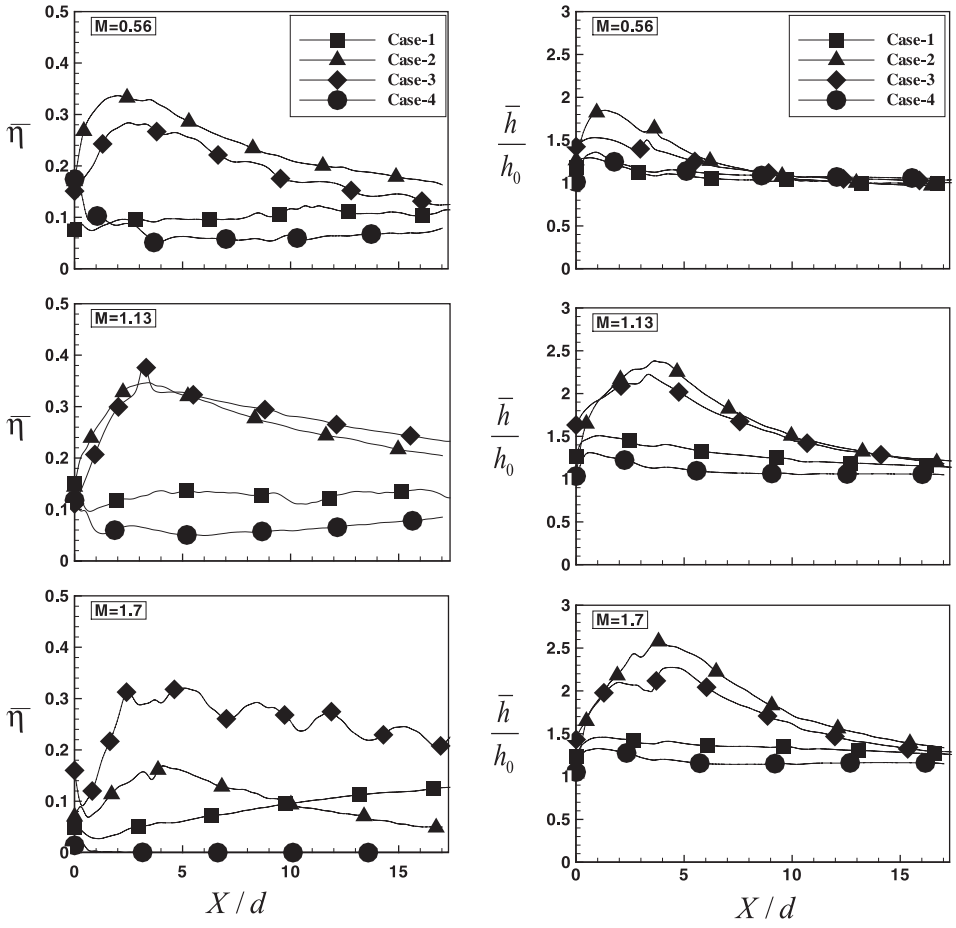

Fig. 10. Effect of tab orientation on span averaged film effectiveness and heat transfer coefficient ratio distributions for all blowing ratios.

one parameter. The results for different density coolant could then be compared under same momentum flux ratio conditions. The density ratio in the present study is closer to 1.0. The heat transfer coefficient ratios and film effectiveness values for all points downstream of the film holes in the measured region are averaged to provide a single area-averaged heat transfer coefficient ratio and film effectiveness value ($0 \leqslant X/d \leqslant 17$). Also presented are heat flux ratio ($\overline{q''}/q''_0$). which integrates the effect of overall-averaged heat transfer coefficient and film-cooling effectiveness values. The heat flux ratios are calculated at every pixel point and averaged as is the case for the heat transfer coefficient and film effectiveness values. Case 2 has the highest $\overline{\overline{\eta}}$ at low I values ($I < 1.3$) but drops off rapidly at high I values ($I = 3$). Case 3 has the highest $\overline{\overline{\eta}}$ value at $I = 3$. Cases 2 and 3 have comparably high ($\overline{\overline{h}}/h_0$) values for the entire I range. Based on these observations, one would expect that Case 3 should provide the lowest heat flux ratio to the plate. This is indeed confirmed by the $\overline{q''}/q''_0$ plot, where Cases 3 and 4 have the lowest heat flux ratio to the surface. The low heat flux ratio for Case 4 (despite the low film effectiveness) is associated with the extremely low values of the heat transfer coefficient obtained for this case (see ($\overline{\overline{h}}/h_0$) plot).

3.3. Discharge coefficients

The discharge coefficients (inversely proportional to the pressure drop across the coolant hole) are plotted in Fig. 12. The discharge coefficients are shown both with and without the cross-flow, and show only a small effect of the cross-flow at low-pressure ratios. There is a significantly larger pressure drop with the downward oriented tabs relative to the horizontal tabs. Since the horizontal tabs had greater effectiveness over the entire range of blowing ratios considered, they are clearly the preferred orientation from the combined perspectives of effectiveness and pressure drop. The downward oriented tabs do provide enhancements in cooling effectiveness, as seen earlier, but this is at the expense of considerably greater pressure drop. The upward oriented tabs do not introduce additional pressure drop across the hole, but as seen earlier, they did not provide any enhancements in film-cooling effectiveness. It is important to note here that the horizontal tabs provide similar levels of

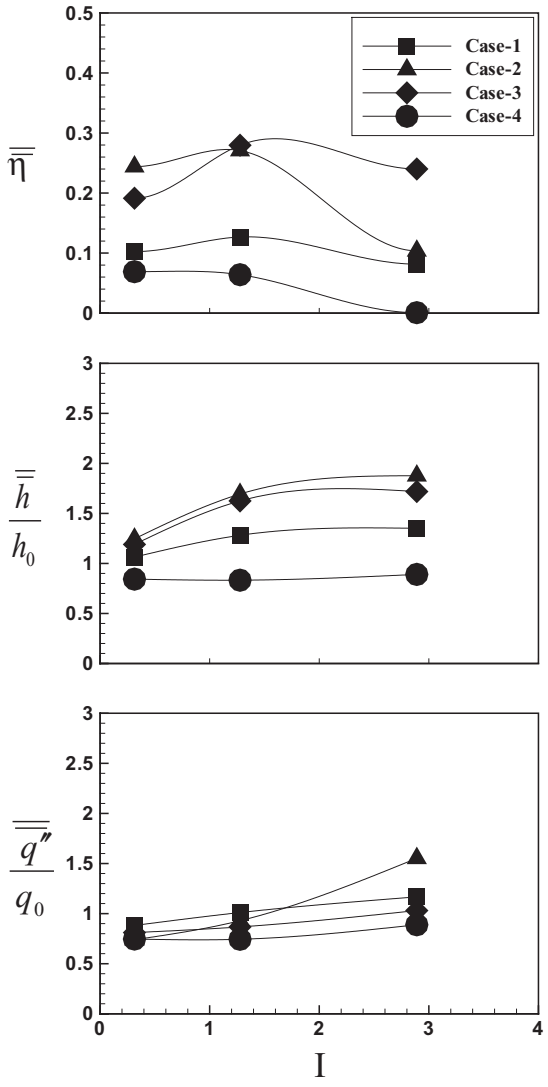

Fig. 11. Effect of momentum flux ratio (I) on overall-averaged film effectiveness, heat transfer coefficient ratio, and heat flux ratio distributions.

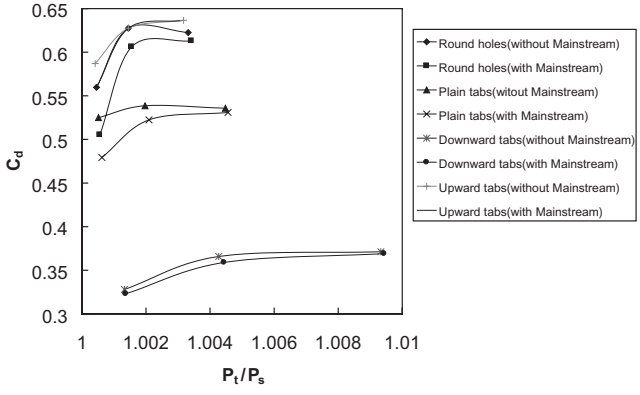

Fig. 12. Effect of tab orientation on discharge coefficients (C_d) with and without cross-flow.

discharge coefficients as that shown by Gritsch et al. (1998b) for their shaped holes at low-pressure ratios. This observation combined with the significantly greater cooling effectiveness achieved with Cases 2 and 3 compared to the baseline case indicate the potential benefits of using tabs to enhance blade cooling.

4. Conclusions

The influence of placing a tab at the exit of a film-cooling hole on the surface heat transfer coefficient and film effectiveness has been investigated. The tabs are located along the upstream edge of the hole. Three different tab orientations have been tested: (1) tabs oriented downward at an angle of −45° (2) tabs placed horizontally parallel to the film cooled surface, and (3) tabs oriented upwards at 45°. The horizontal and downward oriented tabs show the best performance with nearly a threefold enhancement in the peak film-cooling effectiveness for blowing ratios of 1.13 and 1.7. The horizontal tabs appear to exhibit the highest film-cooling effectiveness over the range of blowing ratios tested. The downward oriented tabs exhibit performance comparable to the horizontal tabs at $M = 0.56$ and 1.13, but the performance drops off at the higher blowing ratio of 1.7. The improvements with the horizontal and downward oriented tabs are attributed to the generation of secondary vortices by the tabs with vorticity counter to the kidney pair. This leads to a reduction of the jet penetration and improvement in film-cooling effectiveness. The upward oriented tabs are ineffective, and lead to reductions in the film-cooling effectiveness. For the tabs to be effective, it is observed that they should interact with the flow exiting the film-cooling hole (as for the downward oriented and horizontal tabs) rather than the cross-flow (as for the upward oriented tab). In general heat transfer coefficients are also enhanced (about 40–50%) for horizontal and downward oriented tabs, but the increase in effectiveness (about 200–300%) exceeds the corresponding increase in the heat transfer coefficient. The pressure drop across the hole to provide the same amount of cooling is significantly higher for the downward tabs compared to the horizontal tabs resulting in a greater penalty to achieve higher performance. Since the horizontal tab performance is equivalent to the downward tab and the pressure drop penalty is lower, the horizontal tab is recommended as the best tab configuration.

For engine like conditions, the usage of tabs to improve film cooling may not be a practical solution. It is difficult to apply tabs to actual airfoils as the presence of tabs will increase aerodynamic losses and may also burn off during operation. The present study is aimed at creating better understanding of jet-mainstream mixing and the results may be pertinent to other similar features that may be more practical.

References

Bradbury, L.J.S., Khadem, A.H., 1975. The distortion of a jet by tabs. J. Fluid Mech. 70, 801–813.

Ekkad, S.V., Zapata, D., Han, J.C., 1997a. Heat transfer coefficients over a flat surface with air and CO_2 injection through compound angle holes using a transient liquid crystal image method. ASME J. Turbomach. 119, 580–586.

Ekkad, S.V., Zapata, D., Han, J.C., 1997b. Film effectiveness over a flat surface with air and CO_2 injection through compound angle holes using a transient liquid crystal image method. ASME J. Turbomach. 119, 587–593.

Ekkad, S.V., Nasir, H., Acharya, S., 2000. Film cooling on a flat surface with a single row of cylindrical angled holes: effect of discrete tabs. In: Proceedings of 2000 IMECE, Orlando, Florida.

Eriksen, V.L., Goldstein, R.J., 1974. Heat transfer and film cooling following injection through inclined circular holes. ASME J. Heat Transfer 96, 239–245.

Goldstein, R.J., Taylor, J.R., 1982. Mass transfer in the neighborhood of jets entering a crossflow. ASME J. Heat Transfer 104, 715–721.

Gritsch, M., Schulz, A., Wittig, S., 1998a. Heat transfer coefficient measurements of film cooling holes with expanded slots. ASME Paper No. 98-GT-28.

Gritsch, M., Schulz, A., Wittig, S., 1998b. Adiabatic wall effectiveness measurements of film cooling holes with expanded exits. ASME J. Turbomach. 120, 549–556.

Hay, N., Lampard, D., Saluja, C.L., 1985. Effect of cooling films on the heat transfer coefficient on a flat plate with zero mainstream pressure gradient. ASME J. Eng. Gas Turbines Power 107, 105–110.

Kline, S.J., McClintock, F.A., 1953. Describing uncertainties in single sample experiments. Mech. Eng. 75, 3–8.

Ligrani, P.M., Wigle, J.M., Ciriello, S., Jackson, S.W., 1994a. Film cooling from holes with compound angle orientations: Part 1—Results downstream of two staggered rows of holes with 3d spanwise spacing. ASME J. Heat Transfer 116, 341–352.

Ligrani, P.M., Wigle, J.M., Jackson, S.W., 1994b. Film cooling from holes with compound angle orientations: Part 2—Results downstream of a single row of holes with 6d spanwise spacing. ASME J. Heat Transfer 116, 353–362.

Pedersen, D.R., Eckert, E.R.G., Goldstein, R.J., 1977. Film cooling with large density differences between the mainstream and the secondary fluid measured by the heat-mass transfer analogy. ASME J. Heat Transfer 99, 620–627.

Reiss, H., Bolcs, A., 2000. Experimental study of showerhead cooling on a cylinder comparing several configurations using cylindrical and shaped holes. ASME J. Turbomach. 122, 161–169.

Schmidt, D.L., Sen, B., Bogard, D.G., 1996. Film cooling with compound angle holes: adiabatic effectiveness. ASME J. Turbomach. 118, 807–813.

Sen, B., Schmidt, D.L., Bogard, D.G., 1996. Film cooling with compound angle holes: heat transfer. ASME J. Turbomach. 118, 801–807.

Shih, T.I.-P., Lin, Y.-L., Chyu, M.K., Gogineni, S., 1999. Computations of film cooling from hole with struts. ASME Paper No. 99-GT-282.

Wittig, S., Schulz, A., Gritsch, M., Thole, K.A., 1996. Transonic film cooling investigations: the effect of hole shapes and orientations. ASME Paper No. 96-GT-222.

Zaman, K.B.M.Q., 1998. Reduction of jet penetration in a cross-flow by using tabs. AIAA Paper 98-3276, 34th AIAA/ASME/SAE/ASEE Joint Propulsion Conference & Exhibit, Cleveland.

Zaman, K.B.M.Q., Foss, J.K., 1997. The effect of vortex generators on a jet in a cross-flow. Phys. Fluids 9, 106–114.